A Greedy Algorithm for Optimizing Offshore Wind Transmission Topologies

Stephen Hardy, Hakan Ergun, *Senior Member, IEEE*, and Dirk Van Hertem, *Senior Member, IEEE*

***Abstract*—This work develops a mathematical formulation to determine the combinatorial search space of the Offshore Wind Transmission Optimization Problem (OWTOP). The model accounts for Capital Expenditures (CAPEX), Corrective Maintenance (CM), losses and Expected Energy Not Transmitted (EENT) and determines the optimal radial transmission system topology to connect a number of Offshore Wind Power Plants (OWPPs) to the shore. The model also considers the stochastic nature of wind. In this context a greedy search algorithm is developed capable of finding the globally optimal solution for the location of offshore substations (OSSs), sizing of the transmission infrastructure and topological layout. Rather than a single optimal solution, the algorithm finds a solution space of feasible topologies, bounded from below by the optimal radial solution. The algorithm is applied to 4 test cases including one based on the Belgian North Sea area. It is shown to outperform a traditional Transmission Network Expansion Problem (TNEP) formulation both in computational speed and solution quality.**

***Index Terms*—Wind energy, offshore installations, optimization, greedy algorithms, circuit topology, power transmission.**

NOMENCLATURE

SUB/SUPER-SCRIPTS

Definition	
α	LSB equal to 1
β	Reference bit: $\alpha \leq \beta < \gamma$
c	Complement
cb	Cable
cc	Constrained capacity
ch	Constrained hour
cm	Corrective maintenance
cpx	CAPEX
d	PCC
ens	Energy not served
ex	Exhaustive
fr	Full rank
g	OWPP
γ	MSB equal to 1
h	hour
ls	losses
p	Platform
pk	Peak
pu	per-unit
q	Reactive compensation
sg	Switch-gear
ss	Sub-station
t	Transformer
to	Offshore Transformer
ts	Onshore Transformer
tl	Transmission line
ttl	Total
*	Optimal variation

VARIABLES

Definition	
A	Area
CE_i	Constrained Energy in MWhrs of state i
δ	load loss factor
$C(x)$	cost of equipment x
D	Set of PCCs
G	Set of OWPPs
Λ_x	Availability of x
l_{cb}	Length of a cable in km
η_t	Efficiency of a transformer
λ	Failure rate
g_i	Offshore wind power plant i
μ	Mean time to repair
n_x	Number of equipment x in parallel
O	Set of OSSs
P_i	Probability of state i
Ψ	Power generation time series
q_c	Unit capacitance of c in f/km
Q_c	Total capacitive reactance of c in MVAR
r_c	Unit resistance of c in Ω/km
S_x	Power rating of equipment x in MVA
S_c^q	Compensated cable capacity in MVA
S_{cc}	Constrained capacity in MVA
S_h	Hour h OWPP capacity in MVA
S_{pk}	Peak OWPP capacity in MVA
t_x	Topology of type x
TL	Set of transmission lines

Manuscript received March 3, 2021; revised June 16, 2021 and September 14, 2021; accepted October 10, 2021. Date of publication October 20, 2021; date of current version April 19, 2022. This work was supported by European Union's Horizon 2020 Research and Innovation Programme under the Marie Sklodowska-Curie under Grant 765585. Paper no. TPWRS-00337-2021. *(Corresponding author: Stephen Hardy.)*

Stephen Hardy, Hakan Ergun, and Dirk Van Hertem are with the ELECTA, Department of Electrical Engineering, KU Leuven, Leuven 3000, Belgium, and also with the EnergyVille, Genk, Belgium (e-mail: stephen.hardy@kuleuven.be; hakan.ergun@esat.kuleuven.be; dirk.vanhertem@kuleuven.be).

Color versions of one or more figures in this article are available at https://doi.org/10.1109/TPWRS.2021.3121017.

Digital Object Identifier 10.1109/TPWRS.2021.3121017

U_{ll}	line to line kV
x, y	Spacial coordinates

CONSTANTS

Symbol	Definition (Value)
f	System frequency (50 Hz)
ρ_{cp}	Power density of EEA ($6MW/km^2$) [6]
k_{c_0}	Cost multiplier of laying cable (0.805M€ /km-core) [7]
k_{c_1}	Cost exponent of laying cable (0.985M€ /km-core)
k_{p_0}	Variable cost of a platform (0.085M€ /MVA)
k_{p_1}	Fixed cost of a platform (25M€)
k_{to_0}	Variable cost of an offshore transformer (0.017M€ /MVA)
k_{to_1}	Penalty cost for offshore transformers in parallel (0.25)
k_{ts_0}	Variable cost multiple of an onshore transformer (0.0071)
k_{ts_1}	Variable cost exponent of an onshore transformer (1.05)
k_{ep}	Energy price (50€ /MWh) [8]

Note: for constants not referenced directly a linear regression model was used sourcing data from [7]–[10].

I. INTRODUCTION

IN EUROPE, between 240 and 450GW of offshore wind is needed by 2050 to meet the climate targets agreed upon in The Paris Agreement [1]. As such, the European offshore wind industry is on a course of rapid development for years to come [2] and it is essential that tools for long term planning can also continue to evolve at an equivalent pace.

The Offshore Wind Topology Optimization Problem (OWTOP) describes the problem of optimal planning and expansion of offshore wind transmission networks. Current practice in the industry is to designate regions within national Exclusive Economic Areas (EEAs) for sea based renewable electricity generation. These regions are then divided into concessions which are auctioned off to developers. Developers then optimize concession layout independently. As the industry has matured, however, there has been a realization that savings and increased reliability can be gained if the High Voltage (HV) transmission system topology is planned considering multiple neighbouring concessions [3]–[5]. In the U.K., to incentivize the coordinated development of offshore HV grids and to unbundle transmission and generation, the asset class of Offshore Transmission Owner (OFTO) was created in 2009 [3].

This was done in part to incentivize the development of more coordinated HV grids offshore. Research into the optimal topology of the HV network considering multiple neighbouring concessions is limited [4], [5], [11]. However, much work has been done on the closely related topology optimization problems of collection circuit topology optimization [11]–[25] and the optimal distribution network planning problem [26]–[30].

Topology optimization is an NP-hard problem. As such, heuristics which find a sub-optimal solution in a reasonable time have by far been the most common approach. Genetic Algorithms (GAs) have been the most frequently applied heuristic [5], [11]–[15], but a multitude of other heuristics methods have also been investigated, such as particle swarm [18], simulated annealing [20], modified bat algorithm [19], modified Clark and Wright's savings algorithm [21], minimal spanning tree [22], branch exchange [28] and path search [29]. In addition, classical approaches have been developed. Much progress in convex relaxations has been made [30]–[32] and specific formulations using stochastic programming [23], [24] and Mixed Integer Program (MIP) [25], [33], [34] have been developed. The various problem formulations highlight different problem characteristics and their impact on the overall solution. For example, the importance of accounting for reliability [14], [16], the stochastics of wind speed [23], [24], [35] and optimal locating of Offshore Substations (OSSs) [13], [17], [21] have all been demonstrated.

This work introduces a novel mathematical description of the combinatorial search space and develops an original greedy search algorithm including a proof of global optimality. The presented approach differs from other methods as the transmission system is optimized based on the layout of multiple neighbouring Offshore Wind Power Plants (OWPPs) rather than the Medium Voltage (MV) collection system. This is important as the final turbine locations are not always known during the planning phase of future offshore transmission grids. A real world example of this is occurring in the Belgian North Sea region 2 where the Transmission Service Operator (TSO) is currently planning the Modular Offshore Grid 2 (MOG2) prior to the layout of the individual concessions being finalized [36].

Beyond mostly focusing on the MV network configuration, the main short comings of existing optimization models are a lack of guaranteed optimality or optimality within an overly simplified search space, resulting in a optimal solution from a mathematical perspective but not necessarily from an engineering one.

The proposed solution guarantees global optimality for the physical siting of OSS as well as the selection of transmission infrastructure and the relative topological layout while considering a higher level of detail within the search space compared to alternative approaches. Furthermore, the solution space found includes a ranked set of feasible network topological alternatives bounded from below by the optimal radial topology. This provides designers and planners a rich data set that informs the decision making process far beyond that of a single optimal solution as is the case with comparable alternatives.

To benchmark the model an MIP, Transmission Network Expansion Problem (TNEP) formulation is developed. An MIP was chosen as a guarantee on global optimality can be provided. The implementation of power flow and candidate lines is done with the Powermodels.jl package [37]. This results in both an efficient and fully validated bench-mark with which to compare.

The overall flow of the proposed optimization method is presented in Fig. 1. In the next section the domain and search space are formalized. Following this, a base set of physical topologies which will be input for the greedy search is constructed. Then, the greedy search algorithm is described along with the constraints for achieving global optimality. A proof of global optimality under these constraints is also presented.

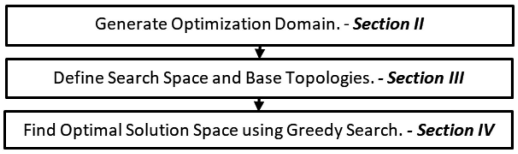

Fig. 1. Overall Steps In Optimization Process.

Finally, results of 4 test cases including the Belgian North Sea area are presented as well as conclusions of the research.

II. Domain and Economic Model

A. Domain

Point of Common Couplings (PCCs), $d_i \in D$, have a connection voltage kV_i^d, a maximum connection capacity, S_i^d, and spacial co-ordinates: xy_i^d. An OWPP, $g_i \in G$, has a generation capacity of S_i^g, a surface area, A_i^g, a power profile Ψ_i^g and spacial co-ordinates, xy_i^g, defining the geographic centre. OWPPs are ordered, 1 to n, by their euclidean distance from the geographic centre to the PCC, where 1 is the OWPP nearest the PCC. The surface area, A_i^g, is found by taking the ratio of S_i^g and ρ_{cp}, the capacity density of the region being modelled.

Ψ_i^g is generated using the CorWind software [38] which combines geographically relevant meteorological data and stochastic simulations to provide generation time series with a per minute resolution. In CorWind meteorological data is obtained from the Weather Research and Forecasting (WRF) model [39] and fluctuations and forecast error are accounted for via the addition of stochastic time series. The resulting time series is translated into an amount of Expected Energy Not Transmitted (EENT) using the Capacity Outage Probability Table (COPT) approach outlined in [40].

Power generated at OWPPs is delivered to a PCC via a topology, consisting of OSSs, $ss_i \in O$, and transmission lines, $tl_{ij} \in TL$. As the topologies are radial, only unidirectional power flow is considered, i.e. from source g_i to demand d_i. MV transmission lines connect OWPPs to OSSs or PCCs and have a capacity and power flow equal to the source g_i as in $S_{ij}^{tl} = S_i^g$ and $\Psi_{ij}^{tl} = \Psi_i^g$. HV transmission lines connect OSSs to OSSs or PCCs. The capacity and power flow in HV transmission lines is similarly determined by its source node ss_i as in $S_{ij}^{tl} = S_i^{ss}$ and $\Psi_{ij}^{tl} = \Psi_i^{ss}$. The capacity and power flow of OSS are determined by taking the sum of all incoming transmission lines as in $S_j^{ss} = \sum S_{ij}^{tl}$ and $\Psi_j^{ss} = \sum \Psi_{ij}^{tl}$.

B. Economic Model

Based on the above, transmission lines and OSS are assigned cables and transformers according to the economic model included in Appendix A. Capital Expenditures (CAPEX), losses, Corrective Maintenance (CM) and EENT are considered.

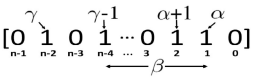

Fig. 2. Notation used for binary representation of OWPPs.

III. Formalized Search Space

A. Formulation

The proposed method uses a combinatorial super set of binary strings to define the exhaustive search space of possible interconnections between OWPPs. Fig. 2 shows an example of the binary representation. Each bit position represents an OWPP. The bit positions begin at zero and proceed to n-1. A bit of value 1, at position i indicates g_i is included within the connection topology. A value of 0 indicates it is not. In order to reference bits in a generalized manner, the following terminology is used. α is the least significant bit that has a value of 1. γ is the most significant bit of value 1. Neighbouring bits to α and γ are indicated via addition and subtraction, but only bits of value 1 are counted as shown in the figure. The third bit reference used is β. β can be any bit position less than γ which is of value 1.

Two classifications of related sets are referred to within this paper. The sets introduced in this section are combinatorial, binary sets. These sets use the notation $\{\boldsymbol{A}\}$ through $\{\boldsymbol{H}\}$ and are a purely mathematical model for abstractly defining the search space. No physical properties are associated to them. Conversely, in Sections III and IV, sets of physical topologies are defined. These sets use the notation $\{\boldsymbol{T_A}\}$ through $\{\boldsymbol{T_H}\}$. The subscripts refer to the related combinatorial set. The term rank is used in reference to the number of OWPPs in a cluster. If 4 OWPPs are connected together to the PCC, the rank is 4. In the case where all OWPPs within a region are connected to the PCC, the term full rank is used. Downstream in a physical topology refers to the direction towards the PCC while upstream is the direction towards the n^{th} OWPP.

B. Combinatorial Super Set

An offshore wind zone consisting of n OWPPs is described by the set of positive integers $\{\boldsymbol{A}\}$ in (1). The set of all possible combinations of at least 1 OWPP is described by $\{\boldsymbol{B}\}$ of (1). $\{\boldsymbol{B}\}$ is the set of n-length binary strings j, spanning from 1 to $2^n - 1$. A value of one only occurs at the bit position equal to i if OWPP g_i is connected within the combination described in j.

$$\begin{aligned} \{\boldsymbol{A}\} &= \{g_i \in \mathbb{Z}_0^+ \mid i < n\}, \\ \{\boldsymbol{B}\} &= \{j \in \mathbb{N}_2^n \mid 0 < j \leq 2^n - 1\} \end{aligned} \tag{1}$$

The decimal equivalent of an element j, can be obtained by taking the sum of products of the bit positions associated with the OWPPs within the combination described by j as in:

$$j = \sum_{g_i \in j} 2^i. \tag{2}$$

For a j containing more than one g_i, it can be decomposed into the sum of two lower valued elements of $\{\boldsymbol{B}\}$ by splitting the binary string at the bit position specified by β as in:

$$j = j_\beta + j_\beta^c,\ j_\beta = \sum_{g_i \in j_\beta} 2^i,\ j_\beta^c = \sum_{g_i \in j_\beta^c} 2^i. \tag{3}$$

However, as each OWPP can only be connected once, a valid decomposition is subject to the constraints:

$$\begin{aligned}&(g_i \in j_\beta) \bigcap (g_i \in j_\beta^c) = \emptyset \text{ and} \\ &(g_i \in j_\beta) \bigcup (g_i \in j_\beta^c) = (g_i \in j).\end{aligned} \tag{4}$$

The set $\{\boldsymbol{C}\}$ of valid elements j_β are found by advancing the bit referenced by β from position α to position γ-1, as in:

$$\{\boldsymbol{C}\} = \{j_{\beta_i}, \forall g_i \in j \mid i < \gamma\} \tag{5}$$

By the same logic as (3), the complementary element j_β^c can be further broken down into maximum n-β components as in:

$$j_\beta^c = \sum_{g_i \in j_1} 2^i + , \ldots , + \sum_{g_i \in j_{n-\beta}} 2^i. \tag{6}$$

The communicative and associative properties of the elements permit components of j_β^c to be re-ordered and re-combined arbitrarily. The set of all valid k-combinations of components is found by enforcing constraints (7b)-(7d) on (7a).

$$\{\boldsymbol{E}\} = \left\{ \binom{\{\boldsymbol{B}\}}{k} \right\} \tag{7a}$$

$$\text{s.t.:} \sum_{j \in k} j = j_\beta^c, j \neq j_\beta^c, \tag{7b}$$

$$\bigcap_{j \in k} (g_i \in j) = \emptyset, \tag{7c}$$

$$\bigcup_{j \in k} (g_i \in j) = (g_i \in j_\beta^c). \tag{7d}$$

Constraint (7b) ensures that the k-combination of components sums to j_β^c while avoiding duplication of the solution of j equal to j_β^c. Constraint (7c) enforces the requirement that an OWPP g_i can only be counted a single time in any topology and (7d) enforces that all OWPPs g_i included in j_β^c are included in the k combination of components. With this definition we are now in a position to define the exhaustive search space by taking the Cartesian product between j_β and $\{\boldsymbol{E}\}$ as in (8). Physically, $\{\boldsymbol{H}\}$ describes all the ways n OWPPs can be interconnected. Describing the interconnections in this manner also provides a clear representation of the indices of iteration. Three nested loops are formed, with k as the inner loop and j the outer loop. Notice, that elements of $\{\boldsymbol{C}\}$ are invariant over the inner loop. This is a key property that is leveraged to ensure the greedy algorithm can achieve global optimality while searching only a fraction of the entire search space.

$$\{\boldsymbol{H}\} = \{j_\beta \times \{\boldsymbol{E}\}\} \mid \forall j_\beta \in \{\boldsymbol{C}\}, \forall j \in \{\boldsymbol{B}\} \tag{8}$$

C. MV and HV Connections

Sets $\{\boldsymbol{A}\}$ through $\{\boldsymbol{H}\}$ describe the combinatorial connection space. They do not contain information regarding the physical properties of the topologies. These characteristics are within the domain of the topological sets described hence forth. A topological set, i.e. $\{\boldsymbol{T_B}\}$, consists of element topologies, t_b. Set $\{\boldsymbol{T_B}\}$ is called the basis set of topologies. It contains at least 1 element for each and every value of j. At times, it is helpful to refer to voltage level specific subsets or topologies, this is done via superscripts. A subset of MV topologies is therefore $\{\boldsymbol{T_B^{mv}}\}$ and a member is t_b^{mv}. For each and every j, a unique t_b^{mv} exists, however, t_b^{hv} only exists if condition (9) is satisfied. In (9), A_α^{mv} is the area of radius l^{mv} surrounding the OWPPs which is closest to the PCC. l^{mv} is the maximum distance MV cable is economic. If (9) is not satisfied, the respective MV topology becomes common to both $\{\boldsymbol{T_B^{hv}}\}$ and $\{\boldsymbol{T_B^{mv}}\}$. Fig. 3 visualizes this for the simplest case of n = 2 OWPPs but is representative of the general case. MV transmission lines are shown in red and HV in black. The red and black dots represent OWPPs and OSSs respectively.

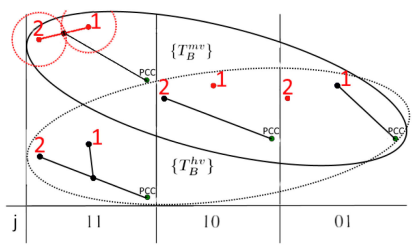

Fig. 3. $\{\boldsymbol{T_B^{hv}}\}$ and $\{\boldsymbol{T_B^{mv}}\}$ for 2 OWPPs.

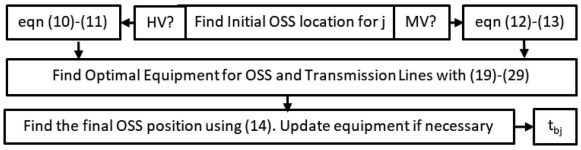

Fig. 4. Flowchart for generating each basis topology t_{b_j}.

$$\begin{aligned}&xy^{ss} \notin A_\alpha^{mv}(l^{mv}) \text{ such that:} \\ &C(cb^{mv})(l^{mv}) = C(ss) + C(sg) + C(cb^{hv})(l^{mv})\end{aligned} \tag{9}$$

The members of $\{\boldsymbol{T_B}\}$ are the simplest variation of MV and HV topologies, having a single OSS as the point of collection for the OWPP feeders. These topologies are the building blocks for topologies generated within the greedy algorithm. What differentiates an MV from an HV topology is the method in which the location of an OSS is determined. Fig. 4 provides an overview of the process of generating a topology t_{b_j}.

1) Initial OSS Placement: The location of the OSS is calculated for each topology by solving a non-linear system, with linear and quadratic constraints. Constraints are generated dynamically and differ between HV and MV topologies. Fig. 3 for j = 11, shows how for the same j, the optimal OSS connection point differs between a MV and HV topology.

a) High Voltage Topology: HV constraint (10) requires an OSS to be placed in the region bounded by the maximum and minimum co-ordinates of the forward most OWPP and the PCC. Region A of Fig. 5 visualizes the constraint. The objective function, (11), minimizes the length of all transmission lines.

$$\begin{aligned}&min(x_\alpha^g, x^d) \leq x \leq max(x_\alpha^g, x^d), \\ &min(y_\alpha^g, y^d) \leq y \leq max(y_\alpha^g, y^d)\end{aligned} \tag{10}$$

$$\min \sum (\|cb^{mv}\| + \|cb^{hv}\|) \tag{11}$$

b) Medium Voltage Topology: MV constraint (12) requires the OSS be placed within the MV economic range of the 2

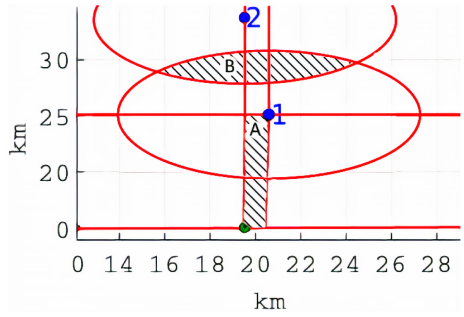

Fig. 5. HV (A) and MV (B) OSS placement constraints.

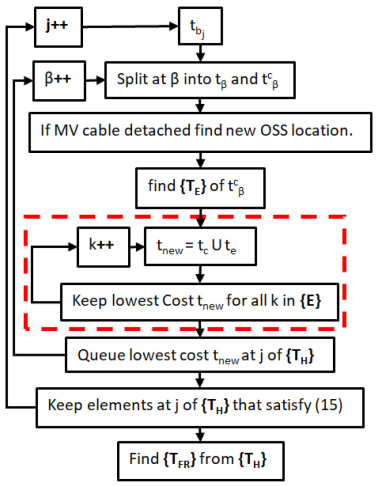

Fig. 6. Greedy Algorithm.

forward most OWPPs while fulfilling objective function (13) of minimizing the length of all MV transmission lines. Region B of Fig. 5 visualizes the constraint.

$$A^{mv}_{\alpha}(l^{mv}) \cap A^{mv}_{\alpha+1}(l^{mv}) \neq \emptyset \tag{12}$$

$$\min \sum \|cb^{mv}\|. \tag{13}$$

2) Topology Optimization: After the initial placement of an OSS, cables and transformers are added to the layout and a cost per unit length in M€ /km for each transmission line is obtained. This permits a final topological optimization by minimizing objective (14) representing the total cost of the system, subject to constraint (12). The solver used is Ipopt [41].

$$\min\left(\sum_{i=1}^{n}(l^{mv}_{cb_i}\cdot C(cb^{mv}_i)) + \sum_{j=1}^{m}(l^{hv}_{cb_j}\cdot C(cb^{hv}_j))\right) \tag{14}$$

IV. Greedy Search

The greedy search algorithm is displayed in Fig. 6. The topologies within the basis set $\boldsymbol{T_B}$ are input and a new topology, t_{new}, is generated for each combination of j, β and k. The position of OSSs remain constant unless a MV cable is among those detached from an export OSS when creating t_c as discussed below. If an MV cable is detached, the new OSS position is calculated by re-solving (14) for $t^{mv}_{b_j}$ after replacing the MV cables to be removed with HV cables. The generation of new topologies, is done via a process of crossing parent topologies, keeping only the successful variations to generate the next generation. This process is comparable to that employed within GAs, however, the process is deterministic and can be guaranteed to find the global optimal under the conditions outlined in Section IV-3.

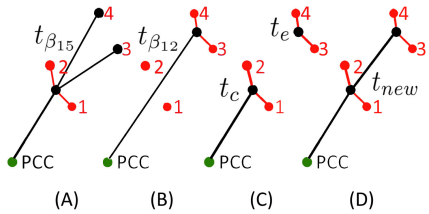

Fig. 7. Crossing topologies for n = 4 OWPPs.

a) Crossing Topologies: The topology t_{new} is the product of crossing 2 component topologies, t_c and t_e. For a desired j, t_c is created by removing all electrical infrastructure in t_b, that is upstream of g_β. It is the topological equivalent of $j_\beta \in \{\boldsymbol{C}\}$. t_e is the complement to t_c and the topological equivalent to $k \in \{\boldsymbol{E}\}$. It is a set of 1 or more topologies, containing all the necessary electrical infrastructure to connect the OWPPs upsteam of g_β and within t_b. t_{new} is created by joining t_e to t_c via OSS to OSS cables as in Fig. 7, which demonstrates this process for a MV topology with j=[1111], β=1 and k=1. In stage (A) and (B), the $\{\boldsymbol{T_B}\}$ topologies for j=[1111], t_{15}, and j=[1100], t_{12}, are shown. In (C) the corresponding components, t_c and t_e are displayed and in (D), the resultant t_{new} is shown after an OSS to OSS cable unifies the component topologies. If the cost of t_{new} is less than t_{15}, it becomes the new resident basis topology.

1) Optimal Topology: $\{\boldsymbol{T_H}\}$ consists of a series of priority queues, one for each value of j. The first element of each queue is the optimal connection topology at j, $t^*_{h_j}$, consisting of a single PCC connection. The length of a queue at j is decided by the number of topologies t_{new} which satisfy condition (15). This condition imposes that for a new topology to be kept, it must be possible to make up the difference in cost between it and $t^*_{h_j}$ by swapping the PCC cable for an OSS to OSS cable.

$$C(t_{h_j} - cb^d_{t_{h_j}}) - C(t^*_{h_j} - cb^d_{t^*_{h_j}}) \leq \frac{\Delta l \cdot C(cb^d_{t^*_{h_j}})}{\left\|cb^d_{t^*_{h_j}}\right\|}, \tag{15}$$

$$\text{where: } \Delta l = \left\| ss^{t^*_{h_j}}_{\alpha} - ss^{t_{h_j}}_{\alpha} \right\|$$

Once $\{\boldsymbol{T_H}\}$ is obtained a set of full rank topologies is calculated as in (16). First, by defining $\{\boldsymbol{T^*_H}\}$ as the set of the lowest cost elements for each priority queue $\{\boldsymbol{T_{H_j}}\}$, and then taking the lowest cost set of k elements within $\{\boldsymbol{T^*_H}\}$.

$$\begin{aligned} &t^* = min(C(t_{fr_k})),\ \forall k \in \{\boldsymbol{T_{FR}}\},\ \text{where} \\ &\{\boldsymbol{T_{FR}}\} = \{\binom{\{T^*_H\}}{k} \mid \textstyle\sum_{\in k} j = 2^n - 1\},\ \text{and} \\ &\{\boldsymbol{T^*_H}\} = \{min(C(t_{h_j}))\ \forall j \in \{\boldsymbol{T_H}\}\}. \end{aligned} \tag{16}$$

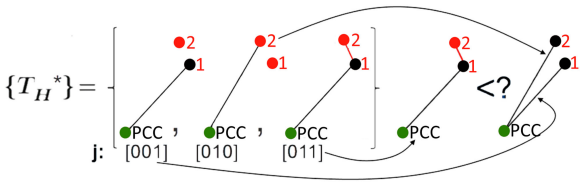

Fig. 8. Example procedure with n = 2 OWPPs for finding the optimal topology with $1 \leq k \leq n$ export cables from $\{\boldsymbol{T_H^*}\}$.

This is visualized in fig 8 visualizes, for the simplest n = 2 OWPPs case.

3) Guaranteeing Optimality: The presented greedy algorithm guarantees global optimality under the condition of a single HV transmission voltage, i.e. OSS to OSS connections are at the same voltage level as OSS to PCC connections. The proof presented here relies on the greedy stays ahead argument [42]. The proof is presented in 2 parts. Part 1 demonstrates that under the assumption that $\{\boldsymbol{T_H^*}\}$ is the set of optimal topologies consisting of k=1 PCC connections, i.e. $\{\boldsymbol{T_H^*}\}=\{t_{h_1}^*, t_{h_2}^*, \ldots, t_{h_m}^*\}$, then t_h^*, the global optimal topology of full rank exists in $\{\boldsymbol{T_{FR}}\}$ and is therefore it's minimum cost member. Part 2 demonstrates that the initial assumption for $\{\boldsymbol{T_H^*}\}$ is in fact true.

Part 1: Given the optimal set of topologies $\{\boldsymbol{T_H^*}\}$ and the condition that no meshed connections are allowed, we can say in general that any topology t_{h_m} consisting of $1 \leq$ k $\leq$ n PCC connections must be the union of k independent topologies, such that $\sum_{\in k} j =$ m and j $\leq$ m. The cost of such a topology would be $C(t_{h_m}) = C(t_{h_{j_1}}) + \cdots + C(t_{h_{j_k}})$ and the cost of the optimal system $C(t_{h_m}^*) = C(t_{h_{j_1}}^*) + \cdots + C(t_{h_{j_k}}^*)$ which is a combination of elements contained within $\{\boldsymbol{T_H^*}\}$ and must therefore be contained within $\{\boldsymbol{T_{FR}}\}$ by definition.

Part 2: We define $\{\boldsymbol{T_H^*}\}$ as the set of partial solutions found by the algorithm and $\{\boldsymbol{T_H^{**}}\}$ as the optimal partial solution set. The goal is to show that for all j $\leq$ m, $C(t_{h_j}^*) \leq C(t_{h_j}^{**})$. This is shown by induction. In the base case where j=1, there is a singular solution and therefore $t_{h_j}^{**} = t_{h_j}^*$. For j>1, we assume it is true for j=m-1 and prove it for j=m. $t_{h_m}^{**}$ is guaranteed to be contained within the exhaustive search space, $\{\boldsymbol{T_H^{ex}}\}$, but not necessarily the reduced greedy search space, $\{\boldsymbol{T_H}\}$. Comparing a single row j of these search spaces, as in (17), we see the reduced search space consists of only the minimal cost topologies of $\{\boldsymbol{T^{hv}}\}_j$ through $\{\boldsymbol{T^{mv}_{\beta_{\gamma-1}}}\}_j$ rather than the full sets.

$$\begin{aligned} &\text{Exhaustive search space:} \\ &\{\boldsymbol{T_H^{ex}}\}_j = \{\{\boldsymbol{T^{hv}}\}_j, \{\boldsymbol{T^{mv}_{\beta_\alpha}}\}_j, \ldots, \{\boldsymbol{T^{mv}_{\beta_{\gamma-1}}}\}_j\} \\ &\text{Greedy algorithm search space:} \\ &\{\boldsymbol{T_H}\}_j = \{t^{hv^{*d}}, t^{mv^{*d}}_{\beta_\alpha}, \ldots, t^{mv^{*d}}_{\beta_{\gamma-1}}\} \end{aligned} \tag{17}$$

It is necessary to demonstrate that the reduction in the search space does not result in the elimination of $t_{h_m}^{**}$. The cost of topology t_m is the sum of the component topology costs, $C(t_{c_m})$ and $C(t_{e_m})$ and the cost of the connection to shore, $C(cb_d)$. Since $C(t_{c_m})$ and $C(cb_d)$ have no dependence on previous topologies, they are unaffected by the reduction in search space for j < m. The dependence on previous topologies is entirely contained within the t_{e_m} term. Thus the dependence can be expressed by the vector equations (18).

Ref	Binaries	Hours
[33]	3000-4000	23.3*
[33]	2000-3000	3.5
[34]	1500-2500	0.75
[34]	1500-2500	0.3

*Author cites memory constraints for high computation time.

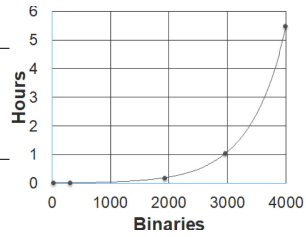

Fig. 9. Typical computation times in state of the art MILP implementations in MV collection circuit optimization for a similar number of binaries (left). Computation times of the TNEP MILP implementation (right).

Observe that $C(\{\boldsymbol{cb_{ss}}\}) - C(\{\boldsymbol{cb_d}\})$ within the boundaries of the queues comprising $\{\boldsymbol{T_H}\}_j$ are constant. They are constant as the locations of the OSSs with which they connect are constant and the required transmission capacity is constant. As such, the order of elements within $\{\boldsymbol{T_E^{ex}}\}_m$ is entirely decided by $\{\boldsymbol{T_H^{ex}}\}_k$. It is therefore, sufficient to retain only the lowest cost topology of each queue, i.e. the reduced search space $\{\boldsymbol{T_H}\}_m$. The same logic applies to any sets k. For systems consisting of more than 1 OSS to OSS connection, part 1 of the proof once again applies with the PCC replaced by a geographically invariant destination OSS. Since the partial solution for every k is optimal we can conclude that the minimum cost topology of the resulting set satisfies the desired criteria of $C(t_{h_m}^*) \leq C(t_{h_m}^{**})$.

$$\begin{aligned} C(\{\boldsymbol{T_E^{hv}}\}_j) = \;& C(\{\boldsymbol{T^{hv}}\}_k + \{\boldsymbol{cb_{ss}}\} - \{\boldsymbol{cb_d}\}) \\ &\vdots \\ C(\{\boldsymbol{T^{mv}_{E\beta_{\gamma-1}}}\}_j) = \;& C(\{\boldsymbol{T^{mv}_{\beta_{\gamma-1}}}\}_k + \{\boldsymbol{cb_{ss}}\} - \{\boldsymbol{cb_d}\}) \end{aligned} \tag{18}$$

V. Results

In existing approaches to the OWTOP, modelling characteristics vary greatly, e.g. sizes of candidate equipment, voltage level, reliability, fixed OSS positions etc. It is therefore difficult to compare the greedy search algorithm directly to other implementations, especially as a majority of implementations focus on the MV collection circuit. Considering this, for the validation of the greedy search algorithm the TNEP formulation of PowerModels.jl [37] is used, which solves the TNEP problem as an underlying MILP. The gurobi solver version 0.9.14 [43] is used for the solution of the MILP problem. To demonstrate the implemented TNEP can be considered representative of the Mixed Integer Linear Program (MILP) class for OWTOPs as a whole, Fig. 9 provides a comparison of the run times of similarly sized state of the art MILP implementations on MV collection circuits and that obtained by our implementation. As the complexity of the problem is strongly linked to the number of binary variables, this is the measure taken for comparing problem size. Note, the number of binaries is not explicitly stated in the original publications and so a range is provided. The run times presented for our implementation include those for the 2, 4 and 6 OWPP test cases as well as two reduced versions of the Belgian north sea presented below.

OWPPs [MW]	
g_1	350
g_2	250

Candidates	
Amount	kV
16	66
8	220
8	400
Total	32

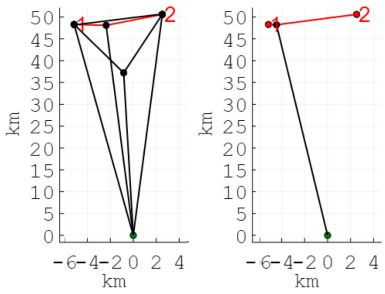

Fig. 10. Case 1: Summary of candidate cables (left). Possible 220 kV connections for 2 OWPPs (centre). Optimal Topology (right).

TABLE I
CASES 2-3 SUMMARY OF OWPP CAPACITIES [MVA]

Case	g_1	g_2	g_3	g_4	g_5	g_6	km*
2	500	600	450	400	-	-	61.6
3	500	600	450	550	400	600	69.2

*Note: Mean OWPP to PCC distance specified.

TABLE II
CASES 1-3 SUMMARY OF RESULTS

Case	Number of OWPPs	Candidate Lines	TNEP [M€]	G.S. [M€]	TNEP [secs]	G.S. [secs]
1	2	32	358.1	357.9	36.1	36.4
2	4	307	1102.4	1103.0	50.2	48.7
3	6	1924	1974.1	1973.6	672.5	67.9

TABLE III
CASE 4 SUMMARY OF BELGIAN OFFSHORE RESULTS

Case	kV	Cb^{hv} [M€]	Cb^{mv} [M€]	Total [M€]	[secs]
GS I	400	392	192.6	1049.3	344*
GS II	220	514.6	205.2	1127.1	349*
GS III	220	519.1	169.7	1142.7	**
TNEP	220	492.5	200.5	1146.7	≈9 days

*Total G.S. time is 693 s the sum of the 400 kV and 220 kV runs. **Computational time included in GSII.

Four test cases are now presented comparing both the TNEP and the proposed greedy search. The first 3 test cases of size 2, 4 and 6 OWPPs are arbitrary regions, while the 4th case is inspired by the Belgian offshore wind concessions. The TNEP is structured as in Fig. 10 for the simple 2 OWPP case. In the centre, the 220 kV candidate grid is depicted. Three OWPP topologies are shown, one with only MV lines connecting to an export OSS, one with only HV lines and one where the 2nd OWPP uses HV and the 1st MV lines. This results in topologies requiring 1, 2 and 3 OSSs. The position of the OSS are optimized as in (14). Direct OWPP to PCC connections are also included. An equivalent 400 kV candidate grid is laid over top, resulting in the total candidate lines shown in the table on the left side of Fig. 10. The right side of Fig. 10 displays the optimal solution consisting of 66 kV connections to a 400 kV export cable.

The remaining cases are modelled in a similar way with the main characteristics of 2 and 3 found in Table I. Table III provides a summary of results from cases 1 to 3. For these 3 cases both methods found the same optimal topology. For the 6 OWPPs case, however, the greedy search arrived at the optimal solution in about $1/10^{th}$ the time.

Test Case 4 - Belgian North Sea: The Belgian offshore region, stage 1, is an area of 238 km^2. The total installed capacity of 2.3 GW is approximated as 8-250 MW OWPPs with geographic centers placed at the coordinates of the existing and planned concessions. The PCC is at the 220 kV substation in Zeebrugge. Wind profile time series are generated using CorWind [38]. The lifespan of the project is considered 25 years at a discount rate of 4% [8].

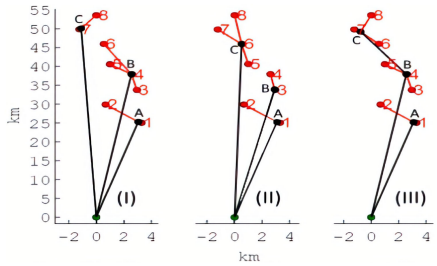

Fig. 11. (I) Optimal Topology. (II) Optimal 220 kV Topology. (III) Topology found in [4].

Comparing this problem size directly to the TNEP model was not possible, as after 15 hours of computation an optimal solution had still not been found. The simulation was terminated at this time with an optimality gap of 21.7% remaining. The incumbent solution at termination time was 1129.5 M€, approximately 8% higher than the value found by greedy search in 693 seconds. As an alternative benchmark, the solution to the identical problem presented in [4] is used. In [4], the region is modelled as a green field sequentially cascading MILP.

Three of the solution topologies found with the greedy algorithm are shown in Fig. 11. The left figure depicts the optimal topology at 400 kV and the centre topology is the lowest cost at 220 kV. The combined computation time for the 400 kV and 220 kV runs was 693 seconds. The results are summarized in Table III.

As the economic models used within this work and that of [4] differ, it is not sufficient to directly compare the objective function values of the optimal solutions. However, as the greedy search finds a hierarchy of solution topologies bounded from below by the optimal solution, it was possible to find the identical topology with greedy search as was found in [4] and compare them directly. This topology is shown on the right side of Fig. 11 at a total cost of 1142.7 M€ . Further details are summarized in Table III. Note that no additional computation time is required to find this topology as it is found simultaneously to the optimal 220 kV solution. The result of [4] using the cost functions in this paper results in a topology cost of 1146.7 M€, an increase of 4 M€ over the identical topology found with greedy search. Although this is a negligible difference, it demonstrates that the quality of the topologies within the greedy search solution space is high. Comparing the results of these two topologies in Table III we see the savings is entirely attributed to reduced cable cost due to OSSs that are better positioned. This is a major advantage of using greedy search and a draw back of the MILP formulation. With finite positions of the OSSs, the optimal location may be missed and the truly optimal topology may be completely eliminated from the search space.

VI. CONCLUSION

Within this work a mathematical framework describing the combinatorial search space of an offshore HV transmission

network was presented. A greedy search algorithm was developed which can find the globally optimal topology given the constraint of using a single HV transmission voltage. The algorithm was then benchmarked against a TNEP formulation for 4 case studies, the last of which is a greenfield representation of the Belgian North Sea area. The greedy search was shown to perform at least as well as the TNEP formulation for small problem sizes of 2 and 4 OWPPs. The developed solution for 6 OWPPs was found in approximately $1/10^{th}$ of the time. For 8 OWPPs the algorithm found the optimal solution in just under 12 minutes while the TNEP formulation failed to converge after 15 hours. In addition to the optimal radial solution, the greedy algorithm provides a ranked set of alternative feasible solutions informing decision makers far better than a single optimal solution.

APPENDIX A

The economic model contained within is based on previous work presented in [40]. The cost of a OSS or PCC, is described by (19). Platform and transformer CAPEXs are given by (20) and (21) respectively, the losses by (22) and EENT by (27). CM for any piece of equipment is a percentage of the acquisition price as specified in Table IV .

TABLE IV
OPEX OF INFRASTRUCTURE AS A PERCENTAGE OF CAPEX [8]

Platform	Transformer	Reactors	Switch Gear	Cable
2.0	0.15	0.15	0.7	2.5

TABLE V
COST OF HVAC REACTORS [8]

Q [MVAR]:	50	75	125	150	200	350
$C_q^{cpx}(Q)$ [M€]:	1.437	2.155	3.595	4.315	5.75	10.065

[0]Note: MVARs for MV cables is assumed to be met by the OWPP generators.

TABLE VI
COST OF SWITCH GEAR [8]

U_{ll} [kV]:	66	220	400
$C_{sg}^{cpx}(U_{ll})$ [M€]:	1.8	3.09	4.545

TABLE VII
EXAMPLE COPT

$\boldsymbol{X}$	$S_{cc,i}$	P_i
1	S	Λ_x
0	0	1-Λ_x

TABLE VIII
RELIABILITY PARAMETERS

Equipment	$\lambda\,[1/yr]$	$\mu\,[months]$
Transformer	0.02	PCC: 0.6, OSS: 3
Cable	0.001/km	2

$$C(ss^{ttl}) = C(p^{cpx}) + C(t^{cpx}) + npv(C(p^{cm}) + C(t^{cm}) + C(t^{eent}) + C(t^{ls})) \quad (19)$$

$$C(p^{cpx}) = \begin{cases} k_{p_0}\left(\frac{S_{ss}+S_t}{2}\right) + k_{p_1} & \text{(Offshore)} \\ 0 & \text{(Onshore)} \end{cases} \quad (20)$$

$$C(t^{cpx}) = \begin{cases} S_t \cdot k_{to_0} \cdot n_t(1 + k_{to_1}(n_t - 2)) & \text{(Offshore)} \\ C(t^{cpx}) = k_{ts_0} \cdot n_t \cdot S_t^{k_{ts_1}} & \text{(Onshore)} \end{cases} \quad (21)$$

$$C(t^{ls}) = 8760 \cdot \delta \cdot k_{ep} \cdot S_t(1 - \eta_t)$$

$$\delta = \sum_{h=1}^{8760}\left(\frac{S_h}{S_{pk}}\right)^2 \Big/ 8760 \quad (22)$$

Cable cost is given by (23)–(25) and (27). The costs of reactive compensation and switch-gear are non continuous functions, shown in Tables V and VI. The tables provide the cost for a single end of the cable. As cable compensation is split 50/50 on either cable end the compensated capacity of the cable is given by (26).

$$C(cb^{ttl}) = C(cb^{cpx}) + 2 \cdot C(q^{cpx}) + 2C(sg^{cpx}) + npv(C(cb^{cm}) + 2C(q^{cm}) + 2C(sg^{cm}) + C(cb^{eent}) + C(cb^{ls})) \quad (23)$$

$$C(cb^{cpx}) = l_{cb} \cdot n_{cb} \cdot C(cb^{pu}) + l_{cb} \cdot n_{cb} \cdot k_{cb_0}(k_{cb_1})^{n_{cb}} \quad (24)$$

$$C(cb^{ls}) = 8760 \cdot \delta \cdot k_{ep}\left(\frac{S_{cb}\eta_t}{\sqrt{3}U_{ll}}\right)^2 \frac{l_{cb} \cdot r_{cb}}{n_{cb}} \quad (25)$$

$$Q_{cb} = 2\pi f \cdot U_{ll}^2 \cdot l_{cb} \cdot n_{cb} \cdot q_{cb},\ S_{cb}^q = \sqrt{S_{cb}^2 - \tfrac{Q_{cb}}{2}^2} \quad (26)$$

EENT is calculated as in (27). For a set of equipment a COPT is built similar to that in Table VII. The number of states, $\boldsymbol{X}$, is equivalent to 2^n, where n is the number of parallel paths. The probability of each state is obtained from (29) and Table VIII. Constrained capacity, S_{cc}, is the capacity remaining after failure.

$$EENT_x = 8760 \cdot k_{ep} \sum_{i \in \boldsymbol{S}} ce_i \cdot P_i. \quad (27)$$

$$ce_i = \sum_{h \in E_{ch}} (S_n - S_{cc_i})$$

$$\text{where } E_{ch} = \{h \in \{1, 2, 3, \ldots, 8760\} \mid S_h > S_{cc_i}\} \quad (28)$$

$$\Lambda_x = \frac{1}{1 + \lambda_x \cdot \frac{\mu_x \cdot 30 \cdot 24}{8760}}, \quad (29)$$

REFERENCES

[1] "Paris agreement to the united nations framework convention on climate change," UNTC XXVII 7.d, Dec. 2015, T.I.A.S. No. 16-1104.

[2] C. Walsh *et al.*, "Wind Europe, Brussels," BE, 2020. [Online]. Available: https://windeurope.org/intelligence-platform/product/wind-energy-in-europe-in-2019-trends-and-statistics/

[3] Cox *et al.*, "Offshore transmission: An investor perspective - Update report," The Office Gas Electricity Markets (OFGEM), London, UK, 2011-99A, Accessed on: Jun. 18, 2020. [Online], Available: https://www.ofgem.gov.uk

[4] S. Hardy *et al.*, "A techno-economic milp optimization of multiple offshore wind concessions," in *The 2nd Int. Conf. Large-Scale Grid Integration Renewable Energy in India*, 2019.

[5] H. Ergun, D. V. Hertem, and R. Belmans, "Transmission system topology optimization for large-scale offshore wind integration," *IEEE Trans. Sustain. Energy*, vol. 3, no. 4, pp. 908–917, Oct. 2012.
[6] Koch, Annika, "European climate, infrastructure and environment executive agency (cinea)," Accessed on: Oct. 28, 2021. [Online]. Available: https://www.msp-platform.eu/practices/capacity-densities-european-offshore-wind-farms
[7] North Seas Countries' Offshore Grid Initiative, "Offshore transmission technology," European Network of Transmission System Operators for Electricity (ENTSO-E), Tech. Rep., 2011.
[8] A. Flament *et al.*, "North sea grid, final report," 3E, DWG, DNV GL, ECN, CEPS, Tech. Rep. 2014.
[9] Navigant Netherlands B. V., "Connecting offshore wind farms," Réseau de Transport d'Électricité and TSO B.V., Tech. Rep., Reference No.: 147432, 2019.
[10] G. Smart, "Offshore transmission benchmarking and cost monitoring," ORE Catapult National Renewable Energy Centre Offshore House, Tech. Rep., 2016.
[11] H. Lingling *et al.*, "Optimization of electrical connection scheme for large offshore wind farm with genetic algorithm," in *Proc. Int. Conf. Sustain. Power Gener. Supply*, 2009, pp. 1–4.
[12] J. Gonzalez, A. Rodriguez, J. Mora, J. Santos, and M. Payan, "A new tool for wind farm optimal design," in *Proc. IEEE Bucharest PowerTech*, 2009, pp. 1–7.
[13] O. Dahmani, S. Bourguet, M. Machmoum, P. Guerin, P. Rhein, and L. Josse, "Optimization of the connection topology of an offshore wind farm network," *IEEE Syst. J.*, vol. 9, no. 4, pp. 1519–1528, Dec. 2015.
[14] O. Dahmani, S. Bourguet, M. Machmoum, P. Guerin, P. Rhein, and L. Josse, "Optimization and reliability evaluation of an offshore wind farm architecture," *IEEE Trans. Sustain. Energy*, vol. 8, no. 2, pp. 542–550, Apr. 2017.
[15] A. M. Jenkins, M. Scutariu, and K. S. Smith, "Offshore wind farm inter-array cable layout," in *Proc. IEEE Grenoble Conf.*, 2013, pp. 1–6.
[16] A. Masmoudi, "2014 ninth international conference on ecological vehicles and renewable energies foreword," *IEEE Trans. Magn.*, vol. 51, no. 4, pp. 1–1, Apr. 2015.
[17] P. D. Hopewell, F. Castro-Sayas, and D. I. Bailey, "Optimising the design of offshore wind farm collection networks," in *Proc. 41st Int. Universities Power Eng. Conf.*, 2006, pp. 84–88.
[18] X. Gong, S. Kuenzel, and B. C. Pal, "Optimal wind farm cabling," *IEEE Trans. Sustain. Energy*, vol. 9, no. 3, pp. 1126–1136, Jul. 2018.
[19] Z. Chen, C. Chen, W. Hu, and P. Hou, "Optimisation of offshore wind farm cable connection layout considering levelised production cost using dynamic minimum spanning tree algorithm," *IET Renewable Power Gener.*, vol. 10, no. 2, pp. 175–183, 2016.
[20] S. Lehmann, I. Rutter, D. Wagner, and F. Wegner, "A simulated-annealing-based approach for wind farm cabling," in *Proc. 8th Int. Conf. Future Energy Syst.*, New York, NY, USA: Association for Computing Machinery, 2017, pp. 203–215. [Online]. Available: https://doi.org/10.1145/3077839.3077843
[21] T. Zuo, Y. Zhang, K. Meng, and Z. Y. Dong, "Collector system topology for large-scale offshore wind farms considering cross-substation incorporation," *IEEE Trans. Sustain. Energy*, vol. 11, no. 3, pp. 1601–1611, Jul. 2020.
[22] Y. Qi, P. Hou, L. Yang, and G. Yang, "Simultaneous optimisation of cable connection schemes and capacity for offshore wind farms via a modified bat algorithm," *Appl. Sci.*, vol. 9, no. 2, pp. 265—285, 2019. [Online]. Available: https://doi.org/10.3390/app9020265
[23] M. Banzo and A. Ramos, "Stochastic optimization model for electric power system planning of offshore wind farms," *IEEE Trans. Power Syst.*, vol. 26, no. 3, pp. 1338–1348, Aug. 2011.
[24] S. Lumbreras and A. Ramos, "A benders' decomposition approach for optimizing the electric system of offshore wind farms," in *IEEE Trondheim PowerTech*, 2011, pp. 1–8.
[25] J. Bauer and J. Lysgaard, "The offshore wind farm array cable layout problem: A planar open vehicle routing problem," *J. Oper. Res. Soc.*, vol. 66, no. 3, pp. 360–368, 2017.
[26] S. Bahadoorsingh, J. V. Milanovic, Y. Zhang, C. P. Gupta, and J. Dragovic, "Minimization of voltage sag costs by optimal reconfiguration of distribution network using genetic algorithms," *IEEE Trans. Power Del.*, vol. 22, no. 4, pp. 2271–2278, Oct. 2007.
[27] D. Jakus, R. aenovi, J. Vasilj, and P. Sarajčev, "Optimal reconfiguration of distribution networks using hybrid heuristic-genetic algorithm," *Energies*, Basel, vol. 13, no. 7, pp. 1544–1565, 2020.
[28] E. Miguez, J. Cidras, E. Diaz-Dorado, and J. L. Garcia-Dornelas, "An improved branch-exchange algorithm for large-scale distribution network planning," *IEEE Trans. Power Syst.*, vol. 17, no. 4, pp. 931–936, Nov. 2002.
[29] V. Kumar *et al.*, "Optimization of radial distribution networks using path search algorithm," *Int. J. Electron. Elect. Eng.*, 2013, doi: 10.12720/ijeee.1.3.182-187.
[30] J. A. Taylor and F. S. Hover, "Convex models of distribution system reconfiguration," *IEEE Trans. Power Syst.*, vol. 27, no. 3, pp. 1407–1413, Aug. 2012.
[31] H. Ergun, J. Dave, D. V. Hertem, and F. Geth, "Optimal power flow for AC-DC grids: Formulation, convex relaxation, linear approximation, and implementation," *IEEE Trans. Power Syst.*, vol. 34, no. 4, pp. 2980–2990, Jul. 2019.
[32] J. Dave, H. Ergun, and D. V. Hertem, "Relaxations and approximations of HVdc grid TNEP problem." in *Proc. 21st Power Syst. Comput. Conf.*, 2020, pp. 1–8.
[33] J.-A. Perez-Rua, M. Stolpe, K. Das, and N. A. Cutululis, "Global optimization of offshore wind farm collection systems," *IEEE Trans. Power Syst.*, vol. 35, no. 3, pp. 2256–2267, May 2020.
[34] J.-A. Perez-Rua, M. Stolpe, and N. A. Cutululis, "Integrated global optimization model for electrical cables in offshore wind farms," *IEEE Trans. Sustain. Energy*, vol. 11, no. 3, pp. 1965–1974, Jul. 2020.
[35] S. Lumbreras and A. Ramos, "Offshore wind farm electrical design: A review: Offshore wind farm electrical design," *Wind Energy*, vol. 16, no. 3, pp. 459–473, 2013.
[36] M. K. Sorensen, "Final study report: MOGII system integration study," Elia Transmission Belgium, DTU Wind Energy, Tech. Rep., 2020.
[37] C. Coffrin, R. Bent, K. Sundar, Y. Ng, and M. Lubin, "Powermodels. JL: An open-source framework for exploring power flow formulations," in *Proc. Power Syst. Comput. Conf.*, 2018, pp. 1–8.
[38] M. Koivisto *et al.*, "Using time series simulation tools for assessing the effects of variable renewable energy generation on power and energy systems," *Wiley Interdiscipl. Reviews: Energy Environ.*, vol. 8, no. 3, pp. e329–344, 2019.
[39] W. C. Skamarock *et al.*, "A description of the advanced research WRF version 4," National Center for Atmospheric Research, Technical Note TN-475+STR, 2019.
[40] S. Hardy *et al.*, "Economic analysis and comparison of options for HVAC, HVDC and OFAC offshore wind power connections," in *Proc. IEEE PES Powertech*, 2019, pp. 1–6.
[41] A. Wachter and L. T. Biegler, "On the implementation of a primal-dual interior point filter line search algorithm for large-scale nonlinear programming," *Math. Program.*, vol. 106, pp. 25–57, 2006.
[42] J. Kleinberg and É. Tardos, *Algorithm Design*. Harlow, U.K.: Pearson Educ. Ltd., 2014, pp. 116–125.
[43] Gurobi Optimization, LLC, "Gurobi optimizer reference manual," 2021. [Online]. Available: http://www.gurobi.com

Stephen Hardy was born in Victoria, Canada, in 1983. He received the B.Eng. degree in electrical engineering from Concordia University, Montreal, QC, Canada, in 2013 and the M.Sc. degree in mathematical modeling from Universitat Autonoma de Barcelona, Barcelona, Spain, in 2017. He is currently working toward the Ph.D. degree with Katholieke Universiteit Leuven, Leuven, Belgium.

Hakan Ergun (Senior Member, IEEE) received the Dipl.-Ing. degree in electrical engineering from the Graz University of Technology, Graz, Austria, in 2009 and the Ph.D. degree from KU Leuven, Belgium, in 2015. He is currently a Research Expert with KU Leuven/EnergyVille, working on transmission expansion planning for large-scale renewable integration, power system security, reliability management, and optimization modelling in power systems. He is the PES Vice Chair of the joint IEEE Benelux IAS/PE/PES Joint Chapter.

Dirk Van Hertem (Senior Member, IEEE) graduated with the M.Eng. degree from KHK, Geel, Belgium, in 2001, the M.Sc. degree in electrical engineering from KU Leuven, Belgium, in 2003, and the Ph.D. degree from KU Leuven, in 2009. In 2010, he was a Member of the EPS Group, Royal Institute of Technology (KTH), Stockholm. Since spring 2011, he has been back to the University of Leuven, where he is currently an Associate Professor with ELECTA Group. His special research interests include decision support for grid operators, power system operation and control in systems with FACTS and HVDC and building the transmission system of the future, including offshore grids and the supergrid concept. The research activities of Prof. Van Hertem are all part of EnergyVille Research Center, where he leads the Electrical Networks activities.